Volume 20 | Number 6 | 7 February 2018 | Pages 691–852

CrystEngComm

rsc.li/crystengcomm

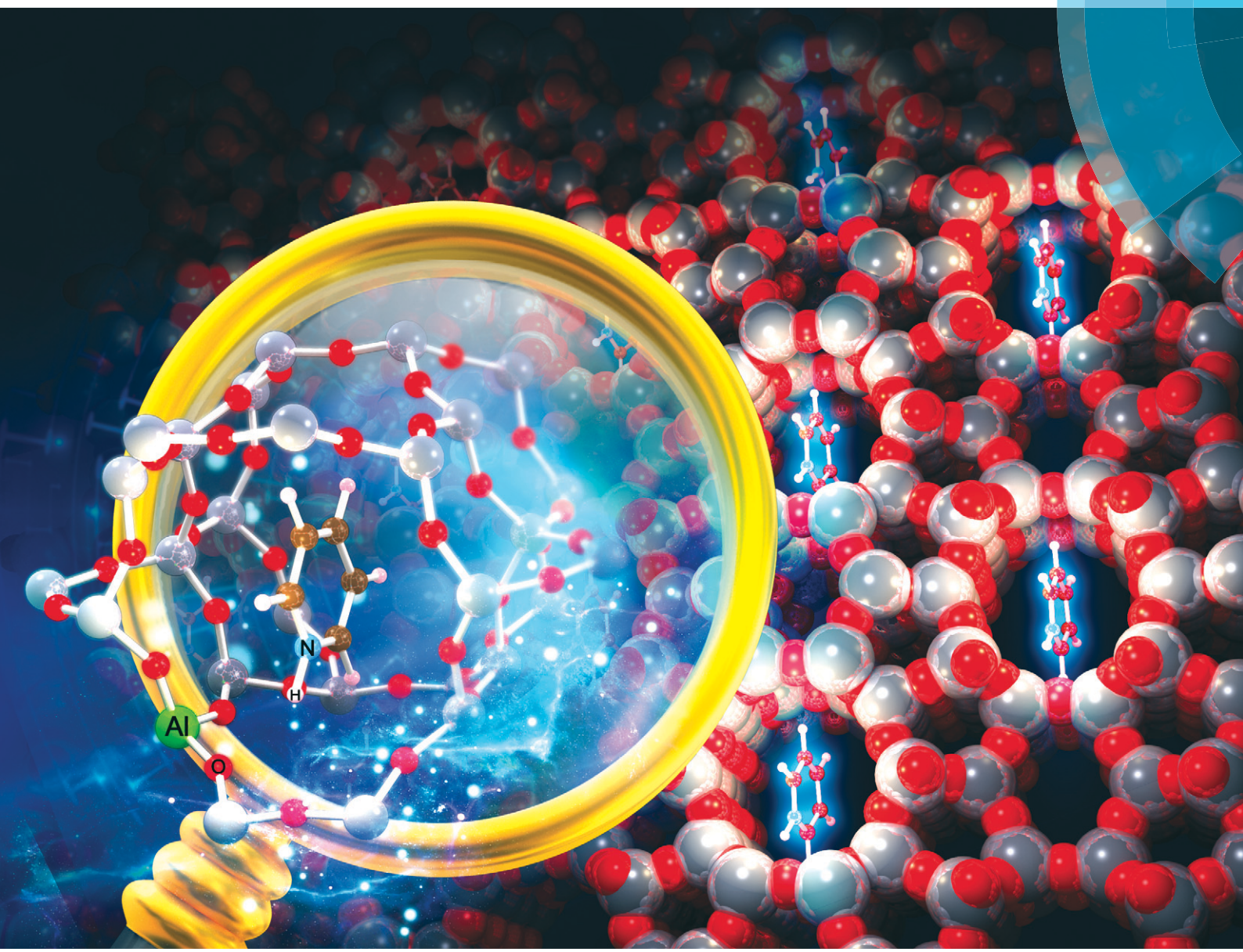

ROYAL SOCIETY OF CHEMISTRY

COMMUNICATION

Peng Guo, Peng Tian, Zhongmin Liu *et al.*

Exploring Brønsted acids confined in the 10-ring channels of the zeolite ferrierite

CrystEngComm

COMMUNICATION

View Article Online
View Journal | View Issue

Cite this: *CrystEngComm*, 2018, **20**, 699

Received 12th November 2017,
Accepted 14th December 2017

DOI: 10.1039/c7ce01967j

rsc.li/crystengcomm

Exploring Brønsted acids confined in the 10-ring channels of the zeolite ferrierite†

Lei Wang, [a] Hongyi Xu, [b] Nana Yan,[ac] Sascha Correll,[d] Shutao Xu,[a] Peng Guo, *[a] Peng Tian*[a] and Zhongmin Liu*[a]

Locations of Brønsted acids confined in the 10-ring channels of ferrierite have been unravelled by refining structural models of as-made and probe-molecule-adsorbed samples against powder X-ray diffraction data, respectively. By analysing both refinement results, it is suggested that Brønsted acid sites can be tailored by controlling the distribution of inorganic ions.

Zeolite, a class of crystalline microporous aluminosilicates, is composed of corner-sharing TO_4 tetrahedra (T = Si, Al) as basic building units. Various arrangements of TO_4 tetrahedra can result in different zeolite frameworks with well-defined cavities or channels of molecular sizes. Until now, the International Zeolite Association-Structure Committee has approved 235 zeolite structures and assigned three-letter codes to them.[1] Zeolites have been widely used in industrial applications such as ion exchange, gas separation, gas storage and organic catalysis.[2–7] The negative charge of the zeolite framework are usually balanced by inorganic cations, organic cations, or both (called structure-directing agents, SDAs) in as-made samples. After calcination, the Brønsted acid, a hydroxyl group bridging Al^{3+} and Si^{4+}, is generated in the proton-form (H-form) sample. Brønsted acid sites (BASs) are one of the most significant parameters influencing the final catalytic performance of zeolites. Therefore, great efforts have been devoted to determining the BASs, including spectroscopy (UV-vis, IR, NMR, and EXAFS),[8–12] probe reactions,[11,13–15] modelling,[12,16–18] *etc.* These approaches either provide limited structural information such as the atomic coordinates of probe molecules (PMs) with respect to the BASs or are challenging to correlate with the specific synthesis parameters (for instance, the silicon source, aluminum sources, and the sequence of reactant mixing). Refinement against X-ray diffraction data is an alternative approach to explore the BASs in specific zeolite structures. Unfortunately, in most cases, zeolites are prone to crystallize in sub-micrometers, even down to nanometers, which is too small to be investigated by the conventional single crystal X-ray diffraction (SCXRD) method. Therefore, Rietveld refinement against powder X-ray diffraction (PXRD) data may be more appropriate for locating the BASs in zeolite structures.

In principle, the BASs could be determined through locating the H^+ or Al^{3+} in the H-form sample directly. However, it is still challenging to determine them by PXRD due to 1) the small scattering factor of H^+, 2) iso-electronic species Al^{3+} and Si^{4+}, and 3) the disordered distribution of H^+ and Al^{3+} in the framework. Alternatively, there are two indirect methods to locate BASs using Rietveld refinement. The first one is to refine the as-made sample in which the SDAs have been occluded in the zeolite. Since Al^{3+} will encircle positive SDAs, probing the interaction between the framework (host) and SDA (guest) might shed light on the BASs. For example, Pinar *et al.* refined the as-made ferrierite (framework type code: **FER**) templated by two kinds of organic SDAs (OSDAs). They found that the interactions between the **FER** framework and OSDAs could provide an indication of the distribution of Al^{3+} in the as-made ferrierites.[19] Another possible method for locating BASs is to refine the PM-adsorbed sample. Zeolites are considered as solid acids, thus, they can interact with basic PMs such as pyridine, generating the classical hydrogen bonding N_{PM}–H···$O_{framework}$. Determining the locations of PMs and exploring interactions between PMs and the framework could indirectly provide evidence of H^+ sites at the atomic level. Recently, the BASs of commercialized H-ZSM-5 (**MFI**) and the ultra-stable zeolite HY (USY, **FAU** topology)

[a] *National Engineering Laboratory for Methanol to Olefins, Dalian National Laboratory for Clean Energy, Dalian Institute of Chemical Physics, Chinese Academy of Sciences, Dalian 116023, P. R. China. E-mail: pguo@dicp.ac.cn, tianpeng@dicp.ac.cn, zml@dicp.ac.cn*
[b] *Inorganic and Structural Chemistry, Department of Materials and Environmental Chemistry, Stockholm University, SE-106 91 Stockholm, Sweden*
[c] *University of Chinese Academy of Sciences, Beijing 100049, P. R. China*
[d] *STOE & Cie GmbH Darmstadt, Hilpertstrasse 10, Darmstadt 64295, Germany*

† Electronic supplementary information (ESI) available: Experimental section, difference electron density map of as-made-FER zeolite, and comparison with other FER zeolites synthesized using different SDAs. CCDC 1578870 and 1578871. For ESI and crystallographic data in CIF or other electronic format see DOI: 10.1039/c7ce01967j

have been unravelled by adsorption of basic PMs and then refining them against synchrotron PXRD to locate the PMs and identify the host–guest interactions.[20,21] Until now, investigations to understand how SDAs influence the distribution of BASs in specific zeolites by Rietveld refinements of both as-made and PM-adsorbed zeolites are still rare.

In this communication, we located the BASs in the **FER** zeolite (2D 10 × 8-ring channel system, Scheme S1†) by refining both as-made and pyridine adsorbed structures against PXRD data. The **FER** framework possesses two distinctive channel systems: the 10-ring channel system along the *c*-axis and the ferrierite cage ($[8^2 6^2 6^4 5^8]$ cavity) with 8-ring pore openings along the *b*-axis (Fig. 1a). The as-made-**FER** zeolite was synthesized by using inorganic Na^+ ions and rigid pyridine molecules. The pyridine-adsorbed sample, H-**FER**-Py, was prepared by the calcination of the as-made-**FER** sample, ammonium exchange, and the adsorption of pyridine molecules at 573 K for 4 hours.

Both field emission scanning electron microscopy (FESEM, Fig. 1b) and PXRD results (Fig. 1c) confirm that the as-made-**FER** is phase pure. The crystals have uniform plate-like morphologies (2 μm × 1 μm × 0.2 μm), as shown in Fig. 1b. The unit cell chemical composition, deduced based on combined results from X-ray fluorescence spectroscopy (XRF) and thermogravimetric analysis (TGA), is $|Na_{1.33}(pyridine)_{3.36}(H_2O)_{2.79}|[Al_{1.33}Si_{34.67}O_{72}]$ (as demonstrated in Table S1 and Fig. S1†). Prior to further investigations, the solid-state ^{13}C NMR clearly indicates the intact structure of occluded pyridine molecules in the as-made-**FER** (Fig. S2†). The equivalent amount of Na^+ and Al^{3+} indicates that the pyridine molecules are not protonated. In order to confirm this result, Fourier transform infrared spectroscopy (FT-IR) of the as-made-**FER** was carried out. It turns out that the crucial band 1540 cm^{-1}, indicating the adsorption of pyridinium ions at Brønsted acid sites (Fig. 1d), is missing.[22] Bands at 1440, 1479, 1579, and 1595 cm^{-1} are assigned to stretching vibrations of the pyridine ring. Although another important band at 1450 cm^{-1}, associated with pyridine coordination at Lewis acid sites, is absent, bands at 1487 and 1624 cm^{-1} might be attributed to the weakly-coordinated pyridine.[22] These results indicate that the rigid and unprotonated pyridine plays a "space-filling" role during the synthesis of zeolites. However, they do not provide sufficient structural information such as the atomic coordinates of SDAs. Fortunately, the good crystallinity of the as-made-**FER** and H-**FER**-Py samples with a relatively high silicon to aluminium ratio (as shown in Fig. S3–S5†) enables us to explore the locations of Na^+ and pyridine through Rietveld refinement.

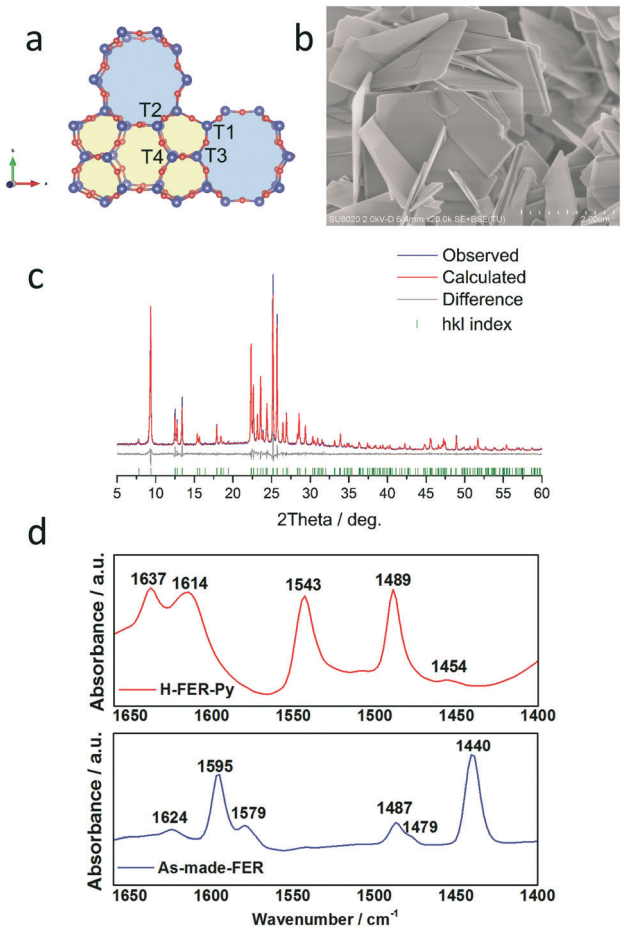

Fig. 1 (a) Framework of the **FER** zeolite (space group: *Immm*) and four non-equivalent T atoms (blue: Al or Si atom, red: O atom). 10-Ring channels and the ferrierite cage are highlighted in light blue and yellow, respectively. (b) A typical SEM image of the as-made-FER sample showing a plate-like morphology. (c) Profile fitting of the as-made-**FER** sample (Cu $K\alpha_1$ radiation λ = 1.5406 Å) and d) FT-IR spectra of the as-made-FER and H-**FER**-Py samples.

The initial atomic coordinates of the zeolite framework are adopted from the idealized **FER** framework deposited in the International Zeolite Association (IZA) – Structure Database.[1] There are four T sites in the asymmetric unit of the **FER** framework with the space group *Immm* (Fig. 1a). Aluminium is treated as being evenly distributed at these four T sites. A thorough examination of the PXRD data of the as-made-**FER** did not reveal any violations in the *Immm* space group. The blue and red curves, as shown in Fig. S6,† are the experimental PXRD data of the as-made-**FER** and the simulated PXRD data of the **FER** framework, respectively. Since high angle data are not affected by guest species in the channel or cavities significantly, the appropriate scale factor between them is calculated using the 2θ range from 40 to 120 degrees. The difference Fourier map is then calculated by applying this scale factor to the whole PXRD pattern (insert in Fig. S6†). It is clear that a cloud of electron density is in the 10-ring channel and the ferrierite cage, corresponding to the positions of pyridines. Furthermore, the isolated electron density highlighted in green (insert in Fig. S6†) indicates the location of Na^+. To retrieve the positions of inorganic Na^+ and organic pyridines accurately, the simulated annealing algorithm, which was initially considered as a direct (real)-space method for structure determination, is employed. Using this approach, Smeets *et al.* have successfully determined the OSDAs in a series of borosilicates.[23] Fixing the **FER** framework and considering pyridine as a rigid body, the initial positions of inorganic and organic SDAs can be located after running a few cycles of the simulated annealing algorithm. The final Rietveld

refinement converged to R_p = 4.261%, R_{wp} = 5.836%, R_{Bragg} = 2.280%, and GOF = 3.256 (Table S2† and Fig. 2a). It is of interest to note that unprotonated pyridines lie in the ferrierite cage parallel to the *ab*-plane (Fig. 2b), while in the 10-ring channel, they are parallel to the *bc*-plane (Fig. 2c). Na^+ ions are only identified in the 10-ring channel, compensating the negative charges from the framework. The Na^+ ion coordinates with framework oxygen atoms O1 and O2 with bond lengths of 2.91(5) Å and 3.16(4) Å, as shown in Fig. 2d, respectively. Among these four T sites in the asymmetric unit, Na^+ is located close to the T1 site, suggesting that the T1 site is the Al^{3+}-rich position.

To confirm the Al^{3+} site and identify the specific oxygen bound to the proton, H-**FER**-Py was prepared (details in the ESI†). The unit cell chemical composition of H-**FER**-Py is also deduced from the XRF and TG results as $|(Hpyridine)_{1.05}(H_2O)_{1.51}|[H_{0.28}Al_{1.33}Si_{34.67}O_{72}]$ (shown in Table S1†). It indicates that 78.94% acid sites could be accessible to PM pyridines based on the unit cell chemical formula. The band at 1543 cm^{-1} in the FT-IR spectrum of the H-**FER**-Py sample, which is associated with the adsorption of pyridinium ions at the BASs, is shown in Fig. 1d. The band at 1454 cm^{-1} indicates that a small amount of pyridine molecules coordinates with the Lewis acid in the framework. It is crucial to determine the positions of the pyridinium ions, which will shed light on the BASs. Thus, Rietveld refinement combined with the simulated annealing algorithm is utilized again to probe the locations of PM pyridinium ions and the host–guest interactions in the H-**FER**-Py sample. The final Rietveld refinement converged to R_p = 5.529%, R_{wp} = 8.258%, R_{Bragg} = 2.529%, and GOF = 5.215 (Table S2† and Fig. 3a). It is worth noting that the pyridinium ions are occluded in the 10-ring channels exclusively (Fig. 3b), while the *fer* cage of the H-**FER**-Py sample is occupied by a guest water molecule, as demonstrated in Fig. 3c. The nitrogen in the pyridine ring was treated to be evenly distributed in the pyridine ring since the nitrogen and carbon cannot be discerned using X-rays directly. In this case, the hydrogen bonding was identified by assuming that the atom in the pyridine closest to a framework oxygen atom is nitrogen.[19,24] After carefully checking the distances between the atoms in pyridine and framework oxygen atoms (Fig. S7†), the shortest distance (N6–H6···O2, 2.987 Å) was identified, as illustrated in Fig. 3b. It indicates the classical hydrogen bonding between the protonated PM pyridine and framework, which is consistent with the IR results. Moreover, the protonated PM pyridine points to the framework oxygen O2, which is associated with the Al^{3+}-rich position T1 as mentioned before. The final Rietveld refinements of the as-made-**FER** and H-**FER**-Py samples show that most of the BASs are i) confined in

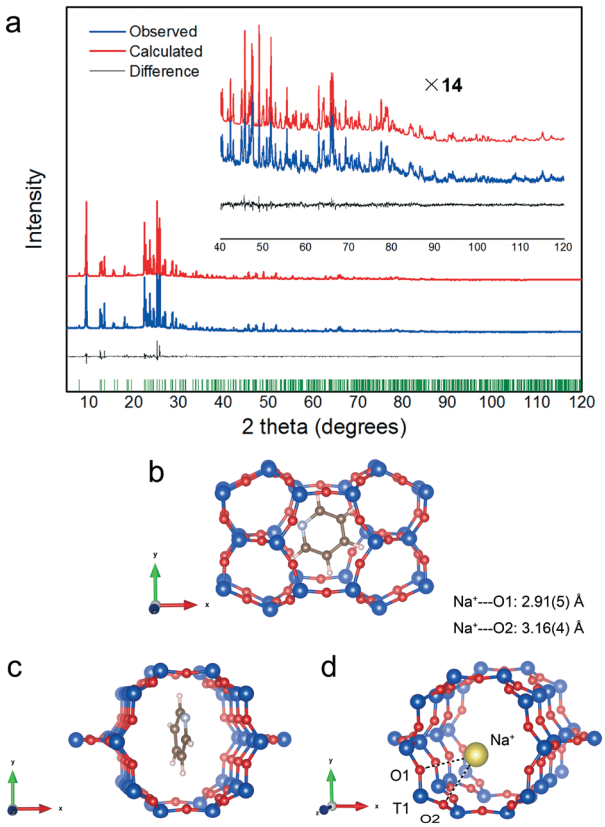

Fig. 2 (a) PXRD Rietveld refinement plots of the as-made-**FER** zeolite (blue: Al or Si atom, red: O atom). The observed, calculated and difference curves are in blue, red and grey, respectively. The vertical bars indicate the positions of Bragg peaks (Cu $K\alpha_1$ radiation, λ = 1.5406 Å). The inset intensities are scaled by a factor of fourteen. The unprotonated pyridine molecules are occluded in the *fer* cage (b) and in the 10-ring channel system (c), respectively. (d) The inorganic sodium cation is in the 10-ring channel.

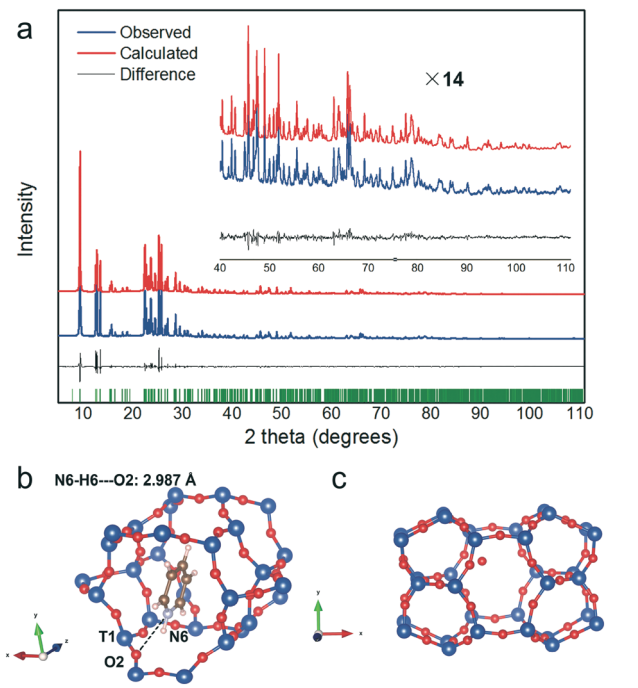

Fig. 3 (a) PXRD Rietveld refinement plots of H-**FER**-Py zeolite (blue: Al or Si atom, red: O atom). The observed, calculated and difference curves are in blue, red and grey, respectively. The vertical bars indicate the positions of Bragg peaks (Cu $K\alpha_1$ radiation, λ = 1.5406 Å). The inset intensities are scaled by a factor of fourteen. (b) Protonated pyridine (pyridinium ions) is occluded in the 10-ring channel system and interacts with framework oxygen through classical hydrogen bonding. (c) The *fer* cage is occupied by a guest water molecule.

the 10-ring channel of the **FER** framework and ii) closely related to the distribution of inorganic Na^+ ions.

In this paragraph, we mainly summarize the locations of Brønsted acids in the **FER** zeolite determined by diffraction methods reported previously as well as in this work (see Table S3,† some studies investigated by IR spectroscopy are also listed). These results are helpful for researchers focusing on the catalysis field. The results provide opportunities for them to choose specific ferrierite zeolites with tailored acid sites. Martucci *et al.* utilized neutron diffraction to locate deuterium atom sites at framework oxygen atoms O3 and O7 in the H-form ferrierite, which was synthesized using pure inorganic cations (Na^+ and K^+) as SDAs. They found that O7 is located towards the *fer* cage while O3 is located in the 8-ring pore opening (Fig. S8a†).[25] Pinar *et al.* refined two as-made samples (named FER-PYRR-TMA and FER-PYRR) against PXRD data, as mentioned in the introduction. It turned out that it is highly possible for protons are to bind to the framework oxygen atoms associated with T1 and T3 in the FER-PYRR-TMA and the FER-PYRR samples, respectively (Fig. S8b and c†).[19] In their previous work, they also confirmed that the FER-PYRR-TMA sample has more BASs in the 10-ring channel system (18% acid sites), becoming more accessible to PM pyridines than FER-PYRR (10%).[15] This is mainly due to the fact that protons, bound to framework oxygen atoms associated with T1 in the FER-PYRR-TMA sample, could be accessed by the PM pyridines. Protons bound to framework oxygen atoms associated with T3 in the FER-PYRR zeolite are embedded in the *fer* cage so that they are inaccessible to PM pyridines.[15] It is worth pointing out that the two samples reported by Pinar *et al.* were synthesized using OSDAs in fluoride medium, while our sample was obtained using the inorganic SDA Na^+ and "space-filling" pyridine molecules in an alkaline medium.[19] The BASs in Pinar's work are controlled by protonated OSDAs, and the ones in our sample are exclusively tailored by inorganic Na^+.

In conclusion, the BASs confined in the 10-ring channel system of the zeolite ferrierite, synthesized using inorganic SDA Na^+ and electrically neutral pyridine molecules, have been determined by refining the as-made-**FER** and H-**FER**-Py structures against PXRD data. This approach, which we proposed in this communication, can be used for probing the acid sites in zeolites as a general method. It can also be extended to other crystalline porous materials such as metal organic frameworks (MOFs) and covalent organic frameworks (COFs). The approach may also provide insights into the tailoring of BASs through the control of SDAs at the atomic level, in turn fulfilling specific catalysis requirements.

Conflicts of interest

There are no conflicts to declare.

Acknowledgements

We acknowledge financial support from the CAS Pioneer Hundred Talents Program (Y706071202).

References

1 Database of Zeolite Structures, http://www.iza-structure.org/databases/, (accessed July 10, 2017).
2 B. M. Weckhuysen and J. Yu, *Chem. Soc. Rev.*, 2015, **44**, 7022–7024.
3 J. Shi, Y. Wang, W. Yang, Y. Tang and Z. Xie, *Chem. Soc. Rev.*, 2015, **44**, 8877–8903.
4 S. H. Cha and S. B. Hong, *J. Phys. Chem. C*, 2017, **121**, 18057–18064.
5 P. Guo, J. Shin, A. G. Greenaway, J. G. Min, J. Su, H. J. Choi, L. Liu, P. A. Cox, S. B. Hong, P. A. Wright and X. Zou, *Nature*, 2015, **524**, 74–78.
6 J. G. Min, K. C. Kemp and S. B. Hong, *J. Phys. Chem. C*, 2017, **121**, 3404–3409.
7 N. H. Ahn, T. Ryu, Y. Kang, H. Kim, J. Shin, I.-S. Nam and S. B. Hong, *ACS Catal.*, 2017, **7**, 6781–6785.
8 S. Bordiga, C. Lamberti, F. Bonino, A. Travert and F. Thibault-Starzyk, *Chem. Soc. Rev.*, 2015, **44**, 7262–7341.
9 J. Dědeček, Z. Sobalík and B. Wichterlová, *Catal. Rev.: Sci. Eng.*, 2012, **54**, 135–223.
10 C. A. Emeis, *J. Catal.*, 1993, **141**, 347–354.
11 T. Yokoi, H. Mochizuki, S. Namba, J. N. Kondo and T. Tatsumi, *J. Phys. Chem. C*, 2015, **119**, 15303–15315.
12 A. Vjunov, J. L. Fulton, T. Huthwelker, S. Pin, D. Mei, G. K. Schenter, N. Govind, D. M. Camaioni, J. Z. Hu and J. A. Lercher, *J. Am. Chem. Soc.*, 2014, **136**, 8296–8306.
13 T. Biligetu, Y. Wang, T. Nishitoba, R. Otomo, S. Park, H. Mochizuki, J. N. Kondo, T. Tatsumi and T. Yokoi, *J. Catal.*, 2017, **353**, 1–10.
14 M. Liu, T. Yokoi, M. Yoshioka, H. Imai, J. N. Kondo and T. Tatsumi, *Phys. Chem. Chem. Phys.*, 2014, **16**, 4155–4164.
15 A. B. Pinar, C. Márquez-Álvarez, M. Grande-Casas and J. Pérez-Pariente, *J. Catal.*, 2009, **263**, 258–265.
16 S. Li, Z. Zhao, R. Zhao, D. Zhou and W. Zhang, *ChemCatChem*, 2017, **9**, 1494–1502.
17 R. Zhao, Z. Zhao, S. Li and W. Zhang, *J. Phys. Chem. Lett.*, 2017, **8**, 2323–2327.
18 R. Karcz, J. Dedecek, B. Supronowicz, H. M. Thomas, P. Klein, E. Tabor, P. Sazama, V. Pashkova and S. Sklenak, *Chem. – Eur. J.*, 2017, **23**, 8987.
19 A. B. Pinar, L. Gómez-Hortigüela, L. B. McCusker and J. Pérez-Pariente, *Chem. Mater.*, 2013, **25**, 3654–3661.
20 B. T. W. Lo, L. Ye, J. Qu, J. Sun, J. Zheng, D. Kong, C. A. Murray, C. C. Tang and S. C. E. Tsang, *Angew. Chem.*, 2016, **128**, 6085–6088.
21 L. Ye, I. Teixeira, B. T. W. Lo, P. Zhao and S. C. E. Tsang, *Chem. Commun.*, 2017, **53**, 9725–9728.
22 E. P. Parry, *J. Catal.*, 1963, **2**, 371–379.
23 S. Smeets, L. B. McCusker, C. Baerlocher, S. Elomari, D. Xie and S. I. Zones, *J. Am. Chem. Soc.*, 2016, **138**, 7099–7106.
24 J. E. Lewis, C. C. Freyhardt and M. E. Davis, *J. Phys. Chem.*, 1996, **100**, 5039–5049.
25 A. Martucci, A. Alberti, G. Cruciani, P. Radaelli, P. Ciambelli and M. Rapacciulo, *Microporous Mesoporous Mater.*, 1999, **30**, 95–101.

